PERGAMON

Journal of Structural Geology 25 (2003) 1281–1299

JOURNAL OF STRUCTURAL GEOLOGY

www.elsevier.com/locate/jsg

# Predicting the three-dimensional population characteristics of fault zones: a study using stochastic models

S.D. Harris*, E. McAllister, R.J. Knipe, N.E. Odling

*Rock Deformation Research, School of Earth Sciences, University of Leeds, Leeds LS2 9JT, UK*

Received 12 November 2001; received in revised form 18 September 2002; accepted 25 September 2002

**Abstract**

Major fault zones are surrounded by damage zones composed of minor faults that, in siliclastic rocks, often form significant barriers to fluid flow. Information on fault damage zone architecture is usually available only as 2D maps, or as 1D line samples or well logs. However, the accurate determination of the 3D fault population characteristics is crucial for flow prediction. In this paper, stochastic models of fault damage zones are generated by incorporating the statistical properties of fault populations (power law length and throw distributions, orientation distribution) and different spatial distributions, including randomly located, simple and hierarchical clustering of faults. These damage zone models are used to investigate the characteristics of 2D and 1D samples, which were found to depend on the 3D power law length exponent, $D_3$, and the spatial distribution of the parent 3D population. Observed 1D samples may fail to show power law characteristics and, therefore, a lack of power law behaviour need not imply a non-power law parent population. The simple rules in which observed 2D and 1D samples follow power laws with exponents $D_2 = D_3 - 1$ and $D_1 = D_3 - 2$, respectively, are not always obeyed. Clustering tends to reduce the difference between these exponents to less than their simple integer values, most markedly for the simple clustering model. The hierarchical clustering model, in which small faults are clustered around larger faults throughout the fault damage zone and which most closely resembles nature, suggests that the simple rule $D_2 = D_3 - 1$ is obeyed with only small deviations but that 1D samples may depart from the simple rule, $D_1 = D_3 - 2$, by as much as 0.25.


*Keywords:* Stochastic models; Fault zones; Flow prediction

## 1. Introduction

Field studies of major fault zones and observations from bore-hole logs and core have shown that major fault zones are surrounded by a ‘damage zone’ of smaller faults. Faults and their damage zones may act as flow conduits or as barriers to flow and frequently determine the distribution of hydrocarbons within a field. The hydraulic properties of faults and their damage zones are therefore of major concern in the hydrocarbon industry. The impact of a fault damage zone on fluid flow depends on the spatial variation in fault rock petrophysical properties, the geometry of the fault network, and particularly on its connectivity, which is controlled by characteristics of the fault size distribution, the fault density and the nature of the fault spatial distribution (Knipe et al., 1997, 1998; Jones et al., 1998). To fully understand connectivity within a fault damage zone, knowledge of the 3D network is required. In recent years the rapid advance in the quality and quantity of seismic data has provided increasingly detailed information on 3D fault networks, but the imaging limitations mean that many minor faults in fault damage zones are still not resolved (below the limit of resolution). Thus, information from fault damage zones is available at best in 2D, in the form of maps derived from outcrops or, more commonly, as 1D line samples provided by well logs and cores. The question of how to predict 3D fault and fracture network characteristics, and particularly hydraulic properties, from 2D and 1D information is therefore an important one (Childs et al., 1990; Heffer and Bevan, 1990).

A number of recent studies (Cowie and Scholz, 1992b; Bour and Davy, 1999; Borgos et al., 2000) have shown that the extrapolation from 1D and 2D information on natural fault populations towards the 3D population is non-trivial. For synthetic populations of faults randomly located in space, simple rules can be used to predict the 3D power law length or throw distribution exponent, by simply adding 2 or

* Corresponding author.
*E-mail address:* sdh@rdr.leeds.ac.uk (S.D. Harris).

0191-8141/03/$ - see front matter © 2003 Published by Elsevier Science Ltd.
PII: S0191-8141(02)00158-X

1 to the 1D or 2D exponents, respectively (Marrett and Allmendinger, 1991). However, in natural cases, spatial distributions are often correlated (e.g. clustered) such that these simple rules can no longer be assumed, and their unguarded use can lead to incorrect predictions of the 3D exponent and, therefore, the fluid flow behaviour (Borgos et al., 2000).

In this paper, we develop a stochastic model of a 3D fault damage zone. This model incorporates statistical properties of fault damage zones observed in outcrop, and includes power law size distributions and a range of spatial distributions from random and uncorrelated to non-random, correlated. This model is then used to examine the effect of the nature of the spatial distribution on the prediction of 3D fault population characteristics from 1D and 2D samples. The results show the importance of the spatial clustering of structures for flow properties and the extent to which the simple rules for extrapolating from 1D and 2D to 3D power law exponents can be in error.

## 2. Fault damage zone characteristics

Several studies in the last 10 years have focused on the architecture of fault damage zones in both crystalline and siliclastic sedimentary rocks and their potential influence on fluid flow (Sibson, 1992; Antonellini and Aydin, 1994, 1995; McGrath and Davidson, 1995; Caine et al., 1996). These studies have been largely field-based and have given insights into the fault network geometry of major faults and their damage zones. In siliclastic sedimentary rocks, faults take the form of deformation bands, along which grain size and porosity are reduced, under sufficient effective stress, to form a partial barrier to fluid flow (Gabrielsen, 1990; Antonellini and Aydin, 1994; Fisher and Knipe, 1998; Aydin, 2000; Shipton et al., 2002). As displacement increases, a group of closely-spaced deformation bands develops until finally a slip surface is formed, along which fault gouge develops and a minor fault zone is formed (Antonellini and Aydin, 1995; Caine et al., 1996; Fossen and Hesthammer, 1997). In such rocks, fault zones are composed of a major slip zone, along which the majority of the displacement occurs, surrounded by a damage zone comprising a complex network of low-throw faults (Antonellini and Aydin, 1995; Shipton and Cowie, 2001). In this paper, two specific examples of major faults in sandstones from England and Utah have been used as the basis for creating a stochastic model of fault damage zone geometry, and their characteristics are summarised below.

### *2.1. Examples of fault damage zones in clastic sediments: the Moab fault, Utah, USA, and the Ninety Fathom fault, England*

The Moab fault in Utah, USA (Foxford et al., 1998) and the Ninety Fathom fault in NE England (Knott et al., 1996) provide well-exposed examples of normal faults and their damage zones in sandstones. The Moab fault is a Tertiary normal fault with a trace length of 45 km and a maximum throw of 960 m, which cuts Jurassic to Cretaceous sandstones and shales of the Paradox Basin, Utah, USA (Foxford et al., 1998). The damage zone of the Moab fault is composed of an anastomosing network of deformation bands, which, in the well-exposed canyon of Bartlett Wash, has an inner zone of well-connected, high density deformation bands 5–12 m thick and an outer damage zone of lower density faults extending up to 60 m into the fault footwall. The damage zone width is defined by the point at which the fault density falls below the background level of one fault per 10 m. Most displacement occurred on a slip zone of anastomosing major slip planes within the inner damage zone. Cumulative fault rock thickness, as measured along 1D traverses in the damage zone, can contribute up to 70% of the total fault rock thickness of the fault zone.

The Ninety Fathom fault in NE England is a dominantly normal fault, which developed in the Devonian (Skamvetsaki, 1994) as the northern boundary of the Northumberland Basin, with a throw of 4–5 km in the basement. It was later reactivated (normal and minor reverse reactivation) in the Mezozoic, with a maximum throw of 260 m (Collier, 1989; Knott et al., 1996). At Cullercoats on the east coast, Permian yellow sands are juxtaposed against Carboniferous shales, and here the fault has a displacement of around 140 m and a damage zone width of around 280 m (Knott et al., 1996). As for the Moab fault, the background fault density defining the boundaries of the fault damage zone is one fault per 10 m (Knott et al., 1996). Like the Moab fault, the Ninety Fathom fault has a complex damage zone of deformation band networks.

#### *2.1.1. Orientation*

In both the Moab and the Ninety Fathom fault damage zones, deformation bands are oriented sub-parallel to the major fault. On linear sections through the Moab fault damage zone, the strike of deformation bands show a Gaussian distribution, with a mean parallel to the major fault and a standard deviation of 10° or less over most of the damage zone. In both the Ninety Fathom (Knott et al., 1996) and Moab faults, the dip distribution is bimodal (conjugate faults), with bands parallel and antithetic to the main fault, having angles of 20–30° between them.

#### *2.1.2. Fault length and throw populations*

In both the Moab and the Ninety Fathom faults, the nature of the outcrop does not allow the determination of the fault length distribution. However, much data on the throw of minor faults and deformation bands has been collected along line sections. For the Moab fault, the frequency–throw graph shows a variable slope but with an overall trend of $-1$ (Fig. 1a). Here, field observations show that the sedimentary layering (beds 0.5–2 m thick) has influenced

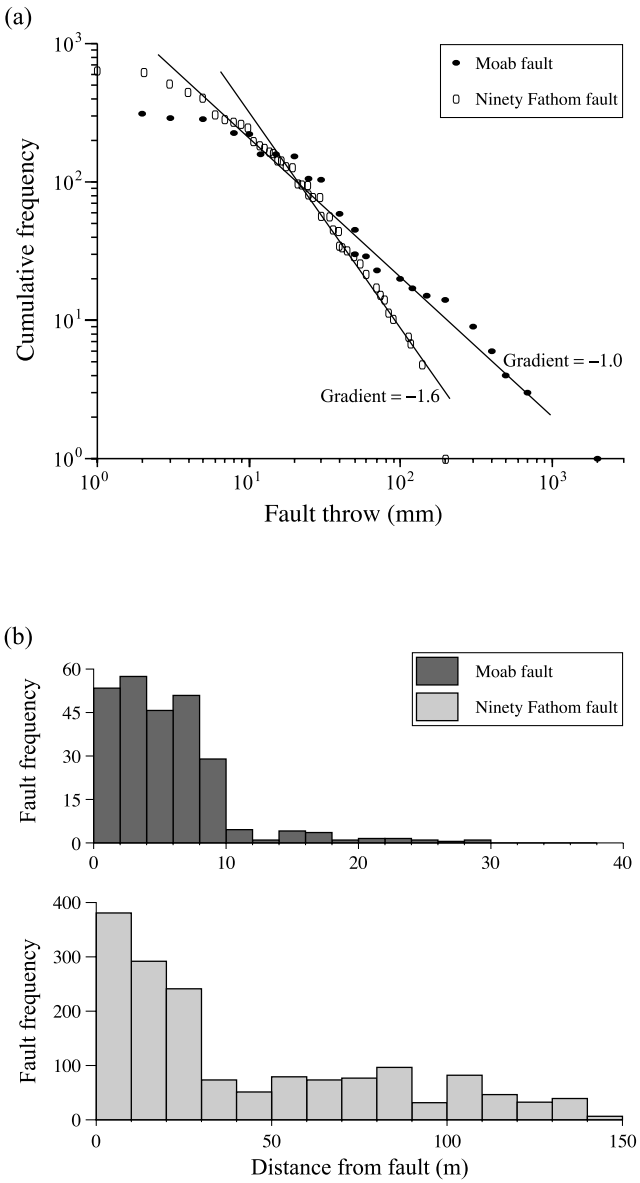


Fig. 1. (a) Fault throw populations and (b) fault frequencies, as a function of distance from the major fault, from the Moab and Ninety Fathom fault zones. Data for the Ninety Fathom fault in (b) is from Knott et al. (1996).

the density and throw distributions of deformation bands, which are often confined to single lithological units. At the Ninety Fathom fault, the rocks of the hanging wall show some subtle sedimentary layering on the scale of centimetres but are otherwise massive sandstones. Deformation band development is therefore less influenced by the sedimentary structure. Here, the cumulative frequency distribution of throws shows an acceptable fit to a power law over about one order of magnitude, with an exponent of around 1.6 (Fig. 1a).

The relationship between fault throw and fault length has been investigated for the Moab Fault. Measurement on outcrop surfaces reveal a wide range in throw to length ratios from 1:100 to 1:1000. Exposed sections through faults that do not pass through fault mid-points are likely to show lower ratios, so that the higher end of the range (1:100) is most likely to represent true fault throw to length ratios.

#### 2.1.3. Fault spatial distribution

In both the Moab and the Ninety Fathoms faults, deformation band density generally increases towards the major slip zone, ranging from 1 to over 100 faults per metre. Fault frequency profiles across the damage zone of both faults show a general increase towards the major slip plane. However, there is significant variation in frequency on the scale of tens of metres and the profiles, although concentrated generally around the major slip zone, are multi-modal (Fig. 1b). The deformation band cumulative frequency distribution of spacing within the damage zone of the Ninety Fathom fault is power law over more than an order of magnitude, with an exponent of around 0.7 (Knott et al., 1996).

## 3. Generation of a fault damage zone stochastic model

### 3.1. Quantification of fault and fault system parameters

In order to make realistic models of fault damage zones, the characteristics of the fault system, including fault size, throw, orientation distributions and the spatial distribution, must be quantified. In addition, correlations between characteristics, such as fault size and throw, and fault size and orientation, must be parameterized. In the following sections, methods for quantitatively describing these characteristics, and how they are incorporated into a model of the fault network within a fault damage zone, are described.

#### 3.1.1. Fault shape and orientation

Observations from seismic surveys indicate that isolated normal faults are planar, with an approximately elliptical shape and a sub-horizontal long axis (Rippon, 1985; Nicol et al., 1996). Nicol et al. (1996) show, from seismic and earthquake data, that fault aspect ratios cover a wide range from 3.5 down to 0.5, and that isolated normal faults show an average aspect ratio of around 2. Greater mechanical anisotropy within the lithological layering restricts fault growth perpendicular to layering, and thus tends to encourage faults with larger aspect ratios. Restricted faults (faults that terminate against other faults) show aspect ratios of around 1.3, or less, for laterally-restricted faults and around 2.5, or more, for vertically-restricted faults. In fault damage zones, faults are intersected by other faults both laterally and vertically, forming a well-connected network, and thus their aspect ratios can be expected to cover a range centred around a ratio of 2. In the model presented in this paper each fault is modelled as a simple elliptical surface with a horizontal long axis of length $l$ and fault ellipse aspect ratios, $r$, that follow a Gaussian frequency distribution, $f(r)$,

with a mean, μ, of 2 and standard deviation, σ, of 0.05:

$$f(r) = \frac{1}{\sqrt{2\pi\sigma^2}} \exp\left[\frac{-(r-\mu)^2}{2\sigma^2}\right]. \quad (1)$$

Here, all minor faults are modelled as ellipses, which is a simplification, but the range of aspect ratios used represents some of the variability found in nature. A more complex model, simulating the physical processes during faulting, would be required to include the effects of restriction by intersecting faults, and thus this approach is viewed as a necessary simplification in the stochastic model.

*3.1.2. Fault throw:length relationship*

Observations of displacement contours on fault planes from seismic and mine data (Rippon, 1985; Nicol et al., 1996) and fault profile data (Dawers et al., 1993) show that the displacement on isolated faults increases from the tip line, which defines the outer edge of the fault, towards its centre. Restricted and complex faults display a basically similar pattern, made more complicated by the presence of other faults (Childs et al., 1995). Displacement profiles of faults show a range from simple pyramid shapes to trapezoidal shapes (pyramid shapes but with a flat top).

Fault length and throw distributions have been widely studied in the literature and widely found to be power law (Childs et al., 1990; Jackson and Sanderson, 1992; Pickering et al., 1996; Steen and Andresen, 1999). For a linear elastic medium, the relationship between fault length and displacement is linear (Pollard and Segall, 1987; Cowie and Scholz, 1992a). In nature, however, power law relationships between fault displacement and length have been found with exponents in the range 0.5–2 (Watterson, 1986; Walsh and Watterson, 1988; Cowie and Scholz, 1992b; Gillespie et al., 1992; Fossen and Hesthammer, 1997). These deviations from a linear relationship are generally thought to be caused by varying mechanical properties of lithological layers together with the linkage and interactions of faults.

In the fault damage zone model presented, a linear relationship between fault length and displacement, as the basic case, is assumed. A simple approach for each model fault, in which displacement increases from zero at the fault tip line to a maximum value at the centre of the fault, is used. The ratio of maximum throw to length can be varied but is set at 1:100 in this paper, which is considered to be the best estimate of average true fault throw to length ratios for siliclastic rocks (Cowie and Scholz, 1992a,b; Dawers et al., 1993; Dawers and Anders, 1995).

*3.1.3. Fault size–frequency distribution*

There is increasing evidence in the literature which shows that fault length distributions determined from map information are frequently power law. A recent review of scaling in fault systems (Bonnet et al., 2001) shows that power law exponents for fault systems range from 0.8 to 1.3 (for the cumulative frequency distribution). There are, unfortunately, no studies of fault length distributions within fault damage zones. However, the Ninety Fathom fault damage zone shows a power law throw distribution with an exponent of around 1.6. Accepting a linear relationship between fault throw and fault length (see Cowie et al., 1996 for a review) thus implies that the fault length distribution is also power law with a similar exponent. Therefore, in the fault damage zone model, it is assumed that the fault plane major axes (fault length) follow a power law. For a power law relationship, the number of faults with lengths greater than or equal to $l$, i.e. the cumulative frequency of faults, $F(l)$, with length at least $l$, is:

$$F(l) \propto l^{-D_3}, \quad (2)$$

where $D_3$ is the three-dimensional power law exponent. In practice, the length population is constrained to lie within the range $l_{min} \leq l \leq l_{max}$, where $l_{min}$ and $l_{max}$ are, respectively, the lower and upper limits of the length scale of interest. If $N$ faults exist over this length range, then the cumulative frequency function (2) can be re-written as follows:

$$F(l) = N\frac{l^{-D_3} - l_{max}^{-D_3}}{l_{min}^{-D_3} - l_{max}^{-D_3}}. \quad (3)$$

The exponent $D_3$ controls the proportion of large to small faults within the population, so that, as $D_3$ is increased towards $D_3 = 3$, small faults become increasingly dominant in the population.

For use in constructing the models, the three-dimensional population of fault size–frequency is described by the cumulative frequency distribution of fault major axis lengths, whose values are drawn randomly from a power law distribution of the form shown in Eq. (3). The process of defining the 3D population of $N$ fault lengths consists of a random sequence of $N$ uniformly distributed values $x \in [0, 1]$. The corresponding length population can then be recovered from the power law definition given in Eq. (3), where the length $l$ is:

$$l = \left[(1-x)l_{max}^{-D_3} + xl_{min}^{-D_3}\right]^{-1/D_3}. \quad (4)$$

*3.1.4. Fault orientation distribution*

The orientation distribution of faults has a strong influence on the connectivity of a fault system. For example, any spatial distribution of faults will be completely unconnected if the faults have identical strikes, dips and plunges (i.e. if they are parallel). The effect of changes in orientation distribution on spatially random systems of fault traces in 2D has been studied by Balberg and Binenbaum (1983) and Robinson (1983), who show that small variations from perfectly parallel fault sets generate significant connectivity. The geometry of deformation bands within the Moab and Ninety Fathom fault damage zones shows that

deformation bands generally have a trend similar to that of the main slip plane (Antonellini and Aydin, 1995; Fossen and Hesthammer, 1997; Shipton and Cowie, 2001), but also show sufficient variation in orientation to generate good connectivity in the sub-horizontal plane. Sub-vertical sections of these damage zones show that the dip of deformation bands can be either unimodal or bimodal, with an angle of 20–30° between the two major dips. Even in the case where dip is unimodal, variations in dip are sufficient to create good connectivity within the vertical plane. In the cases of the Ninety Fathom fault and the Moab fault, the proportion of faults in each of the fault sets where the dips are bimodal is similar. However, in some cases fault may be biased towards one dip direction (e.g. Martel and Boger, 1998).

In the fault damage zone model, the variation in orientation of small faults around larger structures is expressed through the Gaussian distribution similar to Eq. (1), but where $\mu$ is the mean orientation and $\sigma$ its standard deviation, for both the strike and the dip of the fault planes. A Gaussian distribution provides a good description of orientation variations, assuming that the standard deviation of orientation is small (less than about 20°), which is the case for fault damage zones. In the model results presented in this paper, the strike and dip of each fault plane are chosen randomly from separate Gaussian distributions, each with a standard deviation of 10°, following observations from the Moab fault, and with a mean strike parallel to the major slip plane and a mean vertical dip. Thus the models presented here are most representative of fault damage zones in weakly-consolidated clean sandstones.

#### 3.1.5. Spatial distribution

The spatial distribution of faults or fractures is one of the most challenging characteristics to quantify. The various methods that are described in the literature include the analysis of the fault/fracture spacing along 1D sample lines, and the determination of the fractal dimension of the fault/fracture pattern as a whole or of the fault/fracture centre points, or 'barycentres'. Clustering from spacing data along sample lines can be quantified using the coefficient of variation, $C_v$ (standard deviation divided by the mean), where a $C_v$ value of 1 corresponds to a random distribution, $C_v > 1$ to a clustered distribution, and $C_v < 1$ to a spacing distribution more regular than random (Koch and Link, 1970; Odling et al., 1999). There have been numerous attempts at estimating the fractal dimension of fault and fracture systems in the literature. A recent review of this topic (Bonnet et al., 2001) has, however, revealed the pitfalls in the analysis techniques used and the ease with which data can be misinterpreted. Fractal dimensions for 2D maps reported in the literature span the complete possible range of 1–2.

From the point of view of fault and fracture system flow simulation, the main problem with the above methods of quantifying spatial distribution is the difficulty of incorporating them into the simulation models. This is, in part, due to the fact that a fractal dimension or a coefficient of variation only contains a small part of the information required to fully describe the spatial distribution of a fault/fracture system. Other important factors include the correlations between the previously described fault parameters and their position, and variations in fault density in 2D and 3D. Bour and Davy (1999) have found a correlation between fault length and position which shows quantitatively that large faults are more widely spaced than small ones. Due to these difficulties, approaches to simulating fault or fracture spatial distributions rely on geometrical rules for placing faults, after which the simulated patterns can be tested against natural patterns using the analysis techniques described above. In this paper, we explore different methods of simulating clustering in the fault distribution and compare the results with observed outcrop data.

## 4. Simulation of fault system spatial distribution

Due to the difficulty in characterizing spatial distributions of fault networks, many simulation techniques described in the literature have used a Poisson point process, which creates a spatially random distribution in which the location of every fault is independent of all other faults (e.g. Baecher et al., 1977; Long et al., 1982). Over the last few decades, there have also been some attempts at incorporating non-random spatial distributions into models of fault networks (Dershowitz and Einstein, 1988), largely in studies of groundwater flow and contaminant transport. These include the parent–daughter model of Hestir et al. (1987), where 'parent' fault centre points are located in space using a doubly-stochastic Poisson process, producing clustered points, and 'daughter' fault centres are then placed at random distances from the parent centres. Fault planes (discs of random diameter) are then assigned to each centre. This technique was used (Billaux et al., 1989) to simulate a fault system conditioned by observed spatial variations in fault properties. This simulation technique can produce clusters of faults, but does not necessarily cluster small faults around larger ones. Other methods include those used in the 'FracMan' software,[1] which employs the 'nearest neighbour' model, a pattern-based technique, which generates clusters of faults around larger faults, and the 'war zone' model, which simulates shear zones, where clusters of faults are bounded by major faults (Black, 1993; Dershowitz et al., 1998). More recently, Belfield (1998) has developed a technique that builds on fractal concepts and is based on a multifractal strain model in which fault systems are generated using a multiplicative cascade technique with random input from a Lévy-stable distribution. The technique generates a scale-invariant fault network structure

[1] Golder Associates, http://fracman.golder.com

with spacing distributions that range from exponential to power law. At present, this model is 1D only and aimed at reconstructing fault spacing characteristics in bore holes.

In contrast to the above techniques, the stochastic fault network model presented here is specifically aimed at simulating the geological architecture within fault damage zones, as opposed to distributed faulting and fracturing within a rock mass. In order to test the effects of different approaches to clustering on the properties of the fault damage zone model, three types of spatial distribution were generated. These are: (1) a random spatial distribution, where fault centres are randomly located in space and are therefore uncorrelated, (2) a simple clustering model in which faults are preferentially clustered around the main fault or slip plane, and (3) a hierarchical clustering model in which small faults are clustered around a number of the largest faults in the model in addition to the major slip plane. The construction of these spatial models is described below in more detail.

### 4.1. Random spatial distribution of faults

For a given fault population, the random approach locates the centres of each fault independently of all other faults within the population. Clearly, as the fault centres are positioned randomly in three dimensions, we must specify a domain in three-dimensional space within which our population is to be located. This model for spatial distribution, in which the positions of faults are independent and uncorrelated, shows no increase in fault density toward the major slip plane. It does, however, provide a simple case with which to compare the results of the clustered spatial schemes.

### 4.2. Simple clustering—independent location in concentric ellipsoidal shells

In this clustering technique, groups of faults are placed within ellipsoidal shells surrounding the major fault. Thus, each fault is placed independently of any other fault but the density of faults within each ellipsoidal shell may vary. To construct this clustered model, an ellipsoidal volume is created around the major fault whose principal plane and centre coincide with those of the major fault ellipse. This ellipsoid completely encompasses the major fault plane and represents the boundary of the zone containing the centres of all of the clustering faults (Fig. 2a). The volume within this ellipsoid is then divided into a number of concentric ellipsoidal shells (Fig. 2b), so that they cut the principal axis perpendicular to the major fault plane into equal portions. The fault population is then arranged in order of size and divided into groups of equal numbers of faults to be placed inside each shell. The centres of the group of largest faults are first placed within the ellipsoidal shell closest to the major fault and successive groups of faults, of decreasing size, are located in successive shells in a similar fashion. To

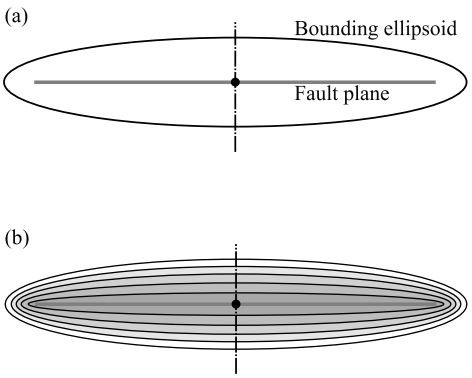


Fig. 2. (a) A section through the ellipsoid defining the boundary of the region around a fault within which all clustered faults are located. (b) Concentric ellipsoidal shells within the ellipsoidal region surrounding the major fault in (a). An equal number of faults is assigned to each shell so that the resulting density of fault centres within each shell decreases with increasing shell size.

place a particular fault centre, $C$, within a shell, a random angle $\phi$ is first used to define a radius within the plane of the major fault slip plane (Fig. 3a). A point $P$ is then chosen at a random location along this radius. The final location of the minor fault centre, $C$, is then chosen at random, within the appropriate shell, along a line normal to the major fault plane through the point $P$ (Fig. 3b). The resulting system of faults shows an increasing fault density (defined as fault area per unit volume) approaching the major slip plane (Figs. 4 and 8b).

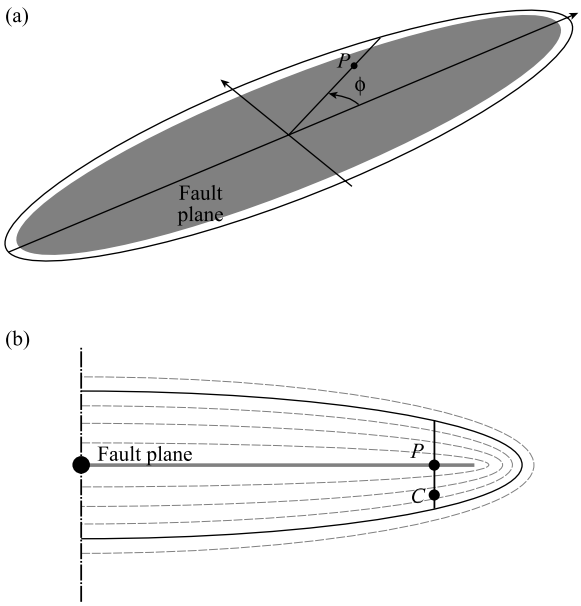


Fig. 3. The location of the fault centre, $C$, for the simple clustering algorithm. (a) The azimuthal angle $\phi$ and the location of $P$ are random within the illustrated bounds. (b) Normal to the radial line containing $P$, the point $C$ is randomly placed within the chosen ellipsoid shell. The simple clustering model shows the most intense clustering around the parent fault centre.

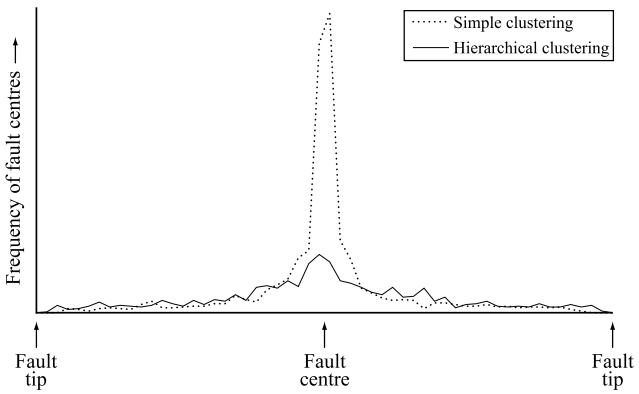


Fig. 4. The variations in the locations of fault centres, relative to the parent fault, for the simple and hierarchical clustering techniques. The total number of clustering faults is the same for each 3D model, but is clearly different along the chosen 1D traverse.

### 4.3. Hierarchical fault clustering technique

The hierarchical fault clustering approach differs from the simple clustering technique by producing spatial clusters of faults at all scales, i.e. for any fault with length greater than that of the smallest fault, $l_{min}$, there is a chance that a smaller fault will be clustered about it. In this model, therefore, the spatial distribution is correlated so that the location of every fault is dependent on the location of all larger faults.

As in the simple clustering technique, the fault population is first arranged in order of size. The major slip plane is used as a starting point for subsequent steps in the algorithm. To place each damage zone fault, a larger, pre-existing fault around which it will cluster is first chosen. The decision of which existing fault to use for the location of the next fault is based upon a cumulative distribution function of the $\alpha$th power of the fault lengths, where the exponent $\alpha$ should typically lie between 1 and 3. The value of $\alpha$ controls the formation of sub-clusters of faults within the damage zone. The larger values of $\alpha$ lead to a higher probability of forming clusters around the very largest faults, while lower values of $\alpha$ will lead to the development of clusters around faults with a broader range of fault lengths.

In the simple clustering model, it was found that the technique used to locate fault centres resulted in a large maximum fault frequency close to the fault centre and along the fault plane minor axis (Fig. 4a). However, field observations on the Moab fault suggest that minor faults in natural fault damage zones are more evenly spread throughout a volume surrounding the main fault and do not cluster so markedly around the major fault centre. In order to spread fault centres more evenly over the parent fault plane, an additional step in the algorithm for the simple clustering model was introduced. This resulted in a flatter frequency profile of clustered minor fault centres, which is thought to be closer to nature (Fig. 4). The algorithm for locating a new fault using the hierarchical fault clustering technique is as follows:

1. We first define an extended ellipse around the major slip plane ellipse (Fig. 5a). A random proportion of the area swept through by a radius of this ellipse is used to define an azimuthal angle $\theta$ and the radius $OP$ (Fig. 5a). The use of the swept area produces a bias towards the major axis of the ellipse in comparison with the use of the random angle (simple clustering technique, Section 4.2), which produces a bias towards the minor axis. A bias towards the major axis is more representative of nature and thus the method of swept area is preferred.
2. A normalised function, $t(r)$, is defined in terms of the normalised distance, $r$, along the radius of the extended ellipse, where $r = 1$ represents the extended ellipse boundary and $r = 0$ is the ellipse centre. The normalised function takes the form shown in Fig. 5b and is defined by the expression:

$$t(r) = \begin{cases} 1 & \text{for } 0 \le r \le p \\ \frac{1}{2}\left(1 + \cos\left[\pi\left(\frac{r-p}{1-p}\right)\right]\right) & \text{for } p \le r \le 1 \end{cases}. \quad (5)$$

   A random value of the integral $\int_0^r t(\bar{r})\mathrm{d}\bar{r}$ of the function (5) is used to define the location $C$ along the radius $OP$ (Fig. 5a and b), with the value $p = 0.2$ being used throughout this paper. This function resembles a pyramid-shaped displacement profile, which has been smoothed and also resembles the displacement profile produced by the Dugdale model (Dugdale, 1960). Thus, the points $C$ are placed with a density variation that reflects strain variations in the immediately adjacent rock mass (Cowie and Scholz, 1992a). This is the extra step added to the simple clustering method that results in minor fault centres spread more evenly over the major fault surface.
3. The point $C$ is used as a starting point for the final steps of the clustering algorithm, which are similar to the simple clustering algorithm explained in Section 4.2. Using the point $C$ as origin, we choose a random (uniform) azimuthal angle $\phi$ and position $D$, located along the resulting chord from $C$ to the extended ellipse boundary (Fig. 5c).
4. Finally, as for the simple clustering model (Section 4.2), the point $F$ in the direction normal to the chosen fault plane is located randomly within an ellipsoid whose minor axis, perpendicular to the fault plane, has a length equal to the maximum fault throw (Fig. 5d). This creates a wider zone of clustered minor faults near the centres of larger faults (Fig. 4).

## 5. Extrapolating from 1D and 2D to 3D—the problem

Fault throw populations, as estimated from 1D samples (i.e. cores, bore hole logs), and fault length populations, estimated from 2D samples (i.e. maps), have been widely reported in the literature. These populations are frequently

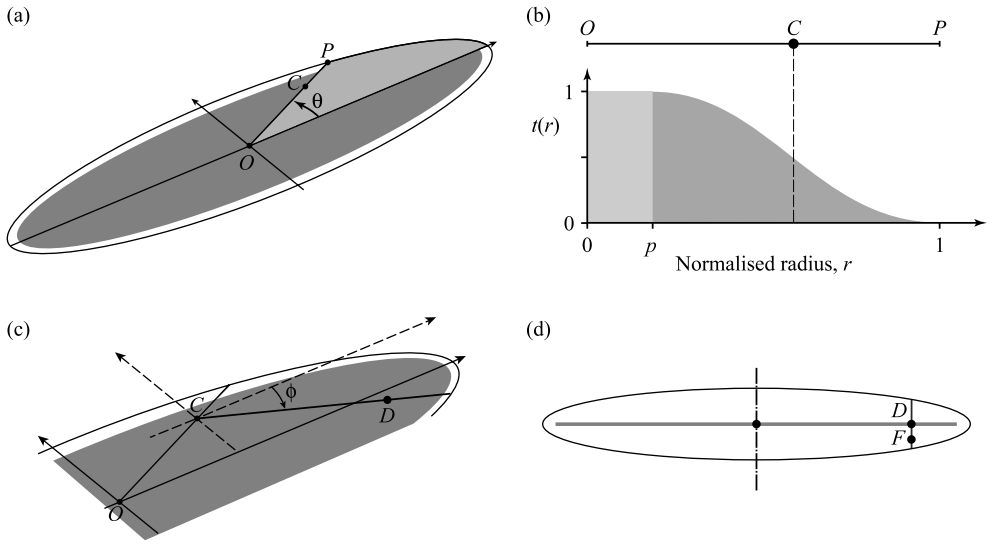


Fig. 5. Illustration of the algorithm for determining the location of the centre of a fault with respect to a chosen larger fault within the hierarchical clustering algorithm: ((a), (b)) radius *OP* is chosen based upon a random area swept around an extended ellipse. The point *C* is chosen along *OP* using a random proportion of the normalised throw as a function *t*; (c) *D* is defined using a random azimuthal angle $\phi$ and a random location along the chord through *C*; (d) the point *F* is placed randomly along a chord normal to the fault plane through *D*. The point *F* acts as the centre for a minor fault clustered around the larger fault.

observed to be power law (e.g. Childs et al., 1990; Scholz and Cowie, 1990; Gillespie et al., 1993; Nicol et al., 1996; Pickering et al., 1996; Watterson et al., 1996; Steen and Andresen, 1999) and suggest that the 1D power law exponent (for the cumulative distribution) lies in the range 0.4–1, whilst the exponent for 2D sampling lies within the range 0.7–1.4 (Bonnet et al., 2001). In the case where fault throw and length are uncorrelated with respect to location, the 3D exponent should be equal to the 1D exponent plus 2 and to the 2D exponent plus 1 (Marrett and Allmendinger, 1991). This will be the case when the spatial distribution of faults is random or follows an isotropic 3D fractal represented by a Sierpinski carpet (Sammis et al., 1986; Gillespie et al., 1993). However, natural fault patterns seldom resemble these simple cases, and so these simple rules need not apply (Cowie and Scholz, 1992b; Bour and Davy, 1999). In particular, different spatial clustering patterns applied to the same 3D population of faults will produce different values of the observed power law exponent when the 3D clustered fault population is subsampled (Borgos et al., 2000).

To illustrate the importance of clustering within populations that have been subsampled, consider the following theoretical example. We suppose that, within a layer-bound stratigraphic sequence, the faults are located such that their centres all lie within a single horizontal plane and that the faults are vertical with horizontal major axes. Then, a 2D subsample using this plane would produce a fault length–frequency power law exponent $D_2$ identical to the original 3D value $D_3$. If, as an extreme example, a line sample through the domain was to pass through these fault centres, then we would predict $D_1 = D_3$. Thus, depending upon the spatial distribution of the faults, the difference $D_3 - D_2$ can lie between 0 and 1, and $D_3 - D_1$ between 0 and 2. In the following sections, the fault damage zone models are used to investigate the effect of different model fault length distributions and spatial clustering techniques on the relationship between the parent 3D population and the fault length and throw distribution characteristics of subsamples measured in 2D and 1D, respectively.

## 6. The effect of size–frequency exponent and spatial distribution on the characteristics of 1D and 2D subsamples

### 6.1. Generating a suite of fault damage zone models

The methods of fault damage zone simulation described in Section 4 are used to create three suites of models with different orientation and spatial distributions. For each of these model types, simulations have been carried out over a range of size–frequency distribution exponents from 1.6 to 2.8. Examples of 2D sections through each of these 3D models, for the case of $D_3 = 2.4$, are shown in Fig. 6, which clearly illustrates the various characteristics of the spatial distribution algorithms. In Fig. 6, the same 80 m (*x*-direction) by 230 m (*y*-direction) section of the plane through the centre of the 3D domain is shown for direct comparison. The first model uses the random spatial distribution with random orientations and shows no higher concentration of faults close to the main slip plane (Fig. 6a). The second model uses the simple clustering technique, so that smaller faults are concentrated near to the main slip plane, and results in a narrow zone of dense faulting (Fig. 6b). By only allowing faults to cluster around the single major fault, the likelihood of sections of large-scale faults being isolated in space with no other faults around them

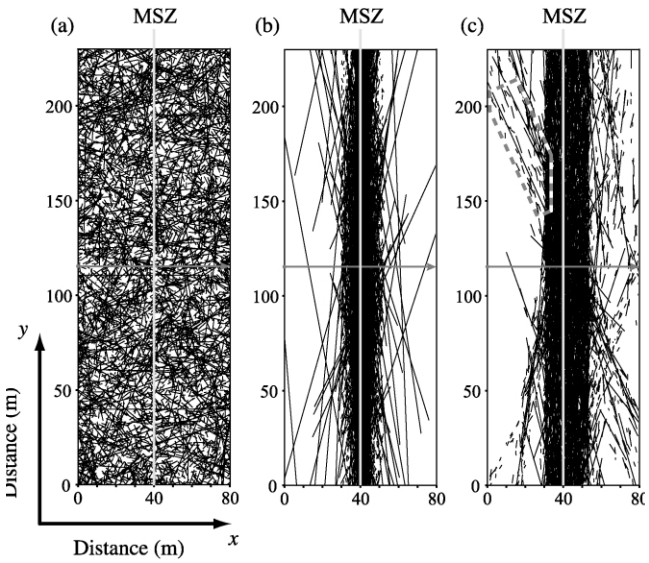


Fig. 6. 2D horizontal slices through the 3D fault arrays produced using (a) random spatial location of all faults (Section 4.1), (b) the simple clustering method of Section 4.2, and (c) the hierarchical clustering method of Section 4.3. For (b) and (c) the slice plane is positioned at the centre of the major fault and the major slip zone (MSZ) is indicated. The regions shown are each 80 m long in the $x$-direction and 230 m long in the $y$-direction. The original domains had the same volume in each case and contained the same number of faults, namely 4.5 million. The grey arrows show the locations of the transects in Fig. 8.

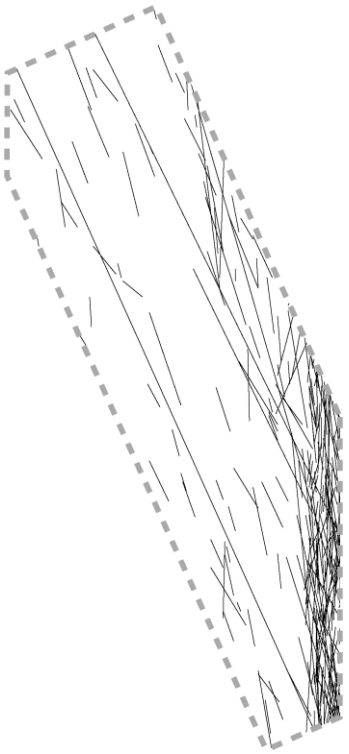

Fig. 7. An enlargement of the region of the fault array highlighted in Fig. 6c, which emphasises the sub-clustering nature of model 3, generated by the hierarchical clustering technique presented in Section 4.3.

exists (Fig. 6b). The third model uses the hierarchical clustering algorithm. In this model, although the initial orientations are chosen from the same Gaussian distributions as for the simple clustering model, the hierarchical clustering scheme generates a broader resultant orientation distribution, which is also approximately Gaussian but less smooth. The resultant pattern for model 3 (Fig. 6c) shows a more spatially-distributed pattern than model 2 (Fig. 6b), since it contains sub-clusters of faults around the larger faults in the damage zone, which are themselves also clustered around the major fault. Fig. 7 shows an enlarged part of Fig. 6c to illustrate this point. The characteristics of these three model types are summarised in Tables 1 and 2.

Using the traverses shown as arrows parallel to the $x$-direction in Fig. 6, the 3D fault arrays are sampled along 1D lines to investigate the spatial distribution and variations in fault density across the models. For the random fault location technique (model 1) shown in Fig. 8a, a relatively low number of faults is sampled across the whole of the 230 m domain. For the distribution of faults in model 2 (simple clustering technique; Fig. 8b) and model 3 (hierarchical clustering technique; Fig. 8c), the highest frequency of faults occurs at the location of the major fault (located at 40 m on the horizontal axis). The distribution is both narrower and the peak at the major fault is higher for model 2 than for model 3. This shows the effect of sub-clustering around other faults within the domain for the hierarchical clustering algorithm. Comparing these frequency distributions across the model fault damage zones with those observed for the Moab and Ninety Fathom faults (Fig. 1b) shows that the hierarchical model (model 3) produces density variations that most closely resemble these examples from nature.

Table 1
Variables used within the three-dimensional fault model for all spatial models

| Fault attributes | Value |
|---|---|
| Maximum fault length, $l_{max}$ (m) | 10,000 |
| Minimum fault length, $l_{min}$ (m) | 2.5 |
| Power law exponent, $D_3$ | 1.6–2.8 |
| Aspect ratio | Gaussian: $\mu = 2$, $\sigma = 0.05$ |
| Plunge angle | 0° |
| Fault throw:length ratio | 1:100 |

### 6.2. Subsampling of model fault populations

The 3D fault damage zone models described above are

Table 2
Characteristics of the three spatial fault damage zone model types

| Model | Spatial model | Orientation |
|---|---|---|
| 1 | Random | Random dip and strike |
| 2 | Simple clustering | Gaussian distribution for dip and strike, $\sigma = 10°$ |
| 3 | Hierarchical clustering | Approximately Gaussian, $\sigma > 10°$ |

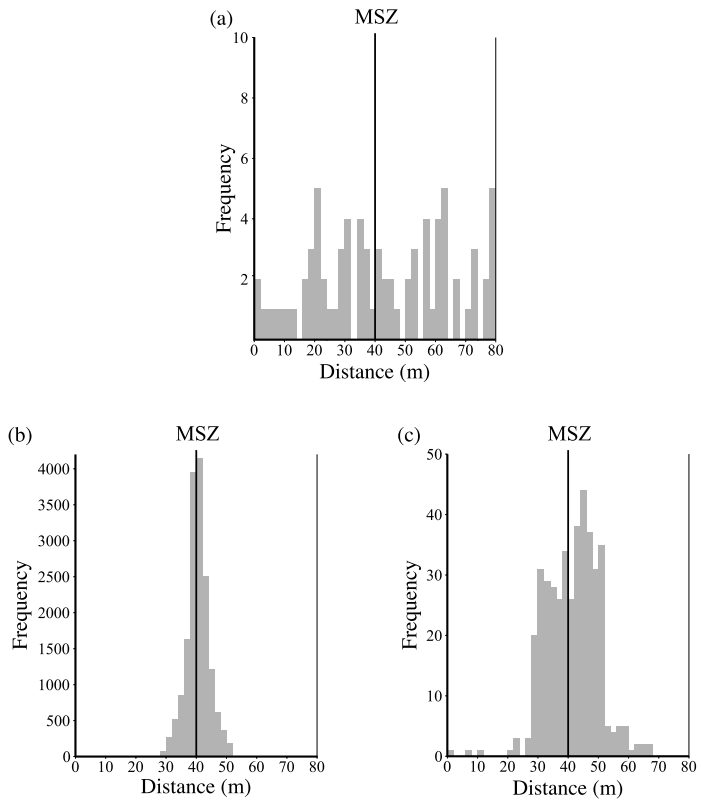


Fig. 8. The frequency of faults along the 1D traverses through the fault damage zone models 1, 2 and 3 displayed in Fig. 6: (a) model 1 (random fault location), (b) model 2 (simple clustering technique), and (c) model 3 (hierarchical clustering technique). Note that the *y*-axis scales vary between each of the three figures and that model 2 produces an extreme clustering around the major fault compared with models 1 and 3. Model 3 produces a pattern that most closely resembles the natural faults (Fig. 1b).

used as a basis for investigating the relationships between the characteristics of 1D and 2D subsamples and those of the parent 3D population. To ensure that the number of subsampled faults at each scale are sufficient to deduce population characteristics, we have populated 3D domains with large samples of $N$ fault lengths, drawn randomly from the appropriate power law cumulative frequency function (Fig. 9). The value of $N$ is an increasing function of $D_3$, since, for larger values of $D_3$, greater numbers of small faults are required before the larger faults in the population are sampled to an acceptable degree. The 3D models constructed contain fault populations of between approximately 2 and 6.5 million faults for $D_3 = 1.6$ to 2.8. Fig. 9 shows that the difference between the model 3D fault population and the original theoretical distribution, as defined by the cumulative distribution function (3), is only apparent for the longer faults lengths close to $l_{max}$. For the example of $D_3 = 2.4$ used in Fig. 9, a fault length within one order of magnitude of $l_{max} = 10{,}000$ m is relatively unlikely to be represented.

The 2D subsamples are taken using horizontal $(x,y)$-planes (perpendicular to the major slip plane) at different $z$ locations within the 3D models. The 1D line samples are taken in the $x$-direction (normal to the major slip plane) at different positions within the $(y,z)$-plane. The locations of these sample planes and lines are illustrated in Fig. 10 for

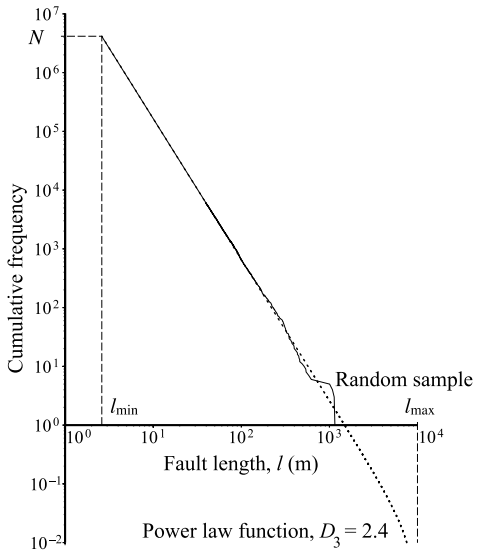


Fig. 9. The cumulative frequency function for $D_3 = 2.4$ (dotted line) and a random sample of $N = 6.5$ million faults drawn from the population of fault lengths (solid line). The theoretical distribution (dotted line) approaches the maximum fault length, $l_{max}$, asymptotically, corresponding to the frequency tending to zero as $l \rightarrow l_{max}$. The random sample follows the theoretical distribution closely up to fault lengths of around 500 m.

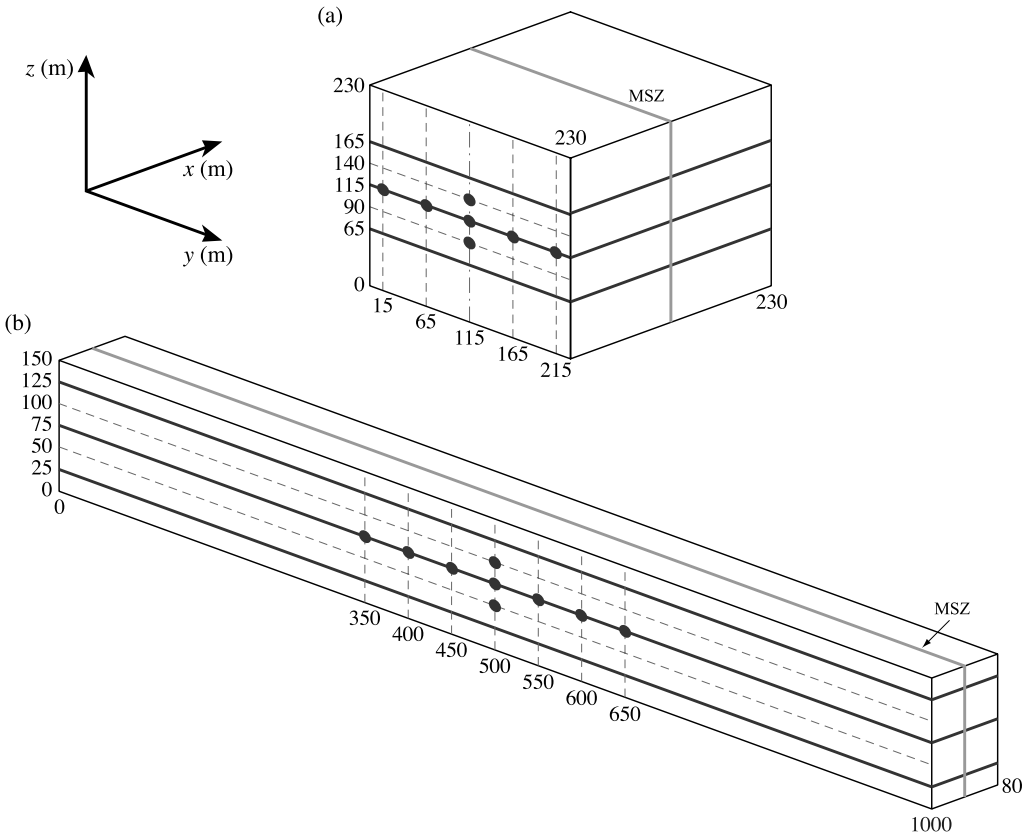


Fig. 10. The locations of the horizontal planes (bold lines) and lines (dots) used to subsample the 3D fault damage zone models. The locations indicated in (a) are for the spatially random fault damage zone model (model 1), using a cubic domain (230 × 230 × 230 m), and the locations indicated in (b) are for the simple and hierarchical clustering techniques (models 2 and 3), for which the domain is cuboid (80 × 1000 × 150 m).

the two different domain sizes, chosen according to whether the fault damage zone model is derived from the spatially random model (model 1; Fig. 10a) or the spatially clustered models (models 2 and 3; Fig. 10b). The three sample planes are located at the centre of the domain, and 50 m above and below this central plane. The line samples lie in the central sample plane at locations separated by 50 m in the $y$-direction, together with additional samples lines 25 m above and below this plane in the $z$-direction.

Based upon the three chosen 3D models of a fault damage zone, the characteristics of the cumulative frequency distribution of fault lengths, $l$, in 2D sections and fault throws, $t$, in 1D sample lines are investigated. These represent fault lengths observed in 2D maps and throw populations observed from displacements of a specific horizon on a high resolution seismic section or from a 1D line sample from outcrop. The results of 1D and 2D subsampling for the case when the 3D fault length distribution is a power law with $D_3 = 2.4$ are shown in Fig. 11. From Fig. 11a, it is clear that both 2D and 1D sections of the 3D model using the random distribution of faults show results that are relatively independent of location. However, for sections from the simple and hierarchical clustering techniques, the numbers of faults sampled and the slope of the graph can vary dramatically according to location, particularly for the 1D sections. These effects are most noticeable for the simple clustering technique (model 2). This model tends to cluster faults close to the centre of the major fault, so that sections passing through this point show the greatest number of faults sampled and the steepest slopes (due to an increased proportion of small faults sampled). This problem is not apparent when the hierarchical clustering technique, which distributes faults more evenly around the major slip plane, is used (model 3) and the 2D subsamples are almost identical for the three locations chosen. The variations seen in this model are, in this case, not due to extreme focusing of faults at the centre of the major fault, but due to the existence of larger sub-clusters of faults located away from the centre of the major fault.

Fig. 11 shows a variety of cumulative frequency trends from curves with significant straight line segments to those where no straight line segment can be identified, and which therefore are not characterized by a power law. The causes of deviation from a straight line for the frequency distribution of a power law population have been extensively discussed in the literature. These include truncation effects, where, due to limited resolution, small faults are under-represented, and censoring effects, where, due to the finite size of the samples, large faults are under-sampled (Lindsey and Rothrock, 1995; Pickering et al., 1995; Odling, 1997; Bour and Davy, 1999). These effects produce

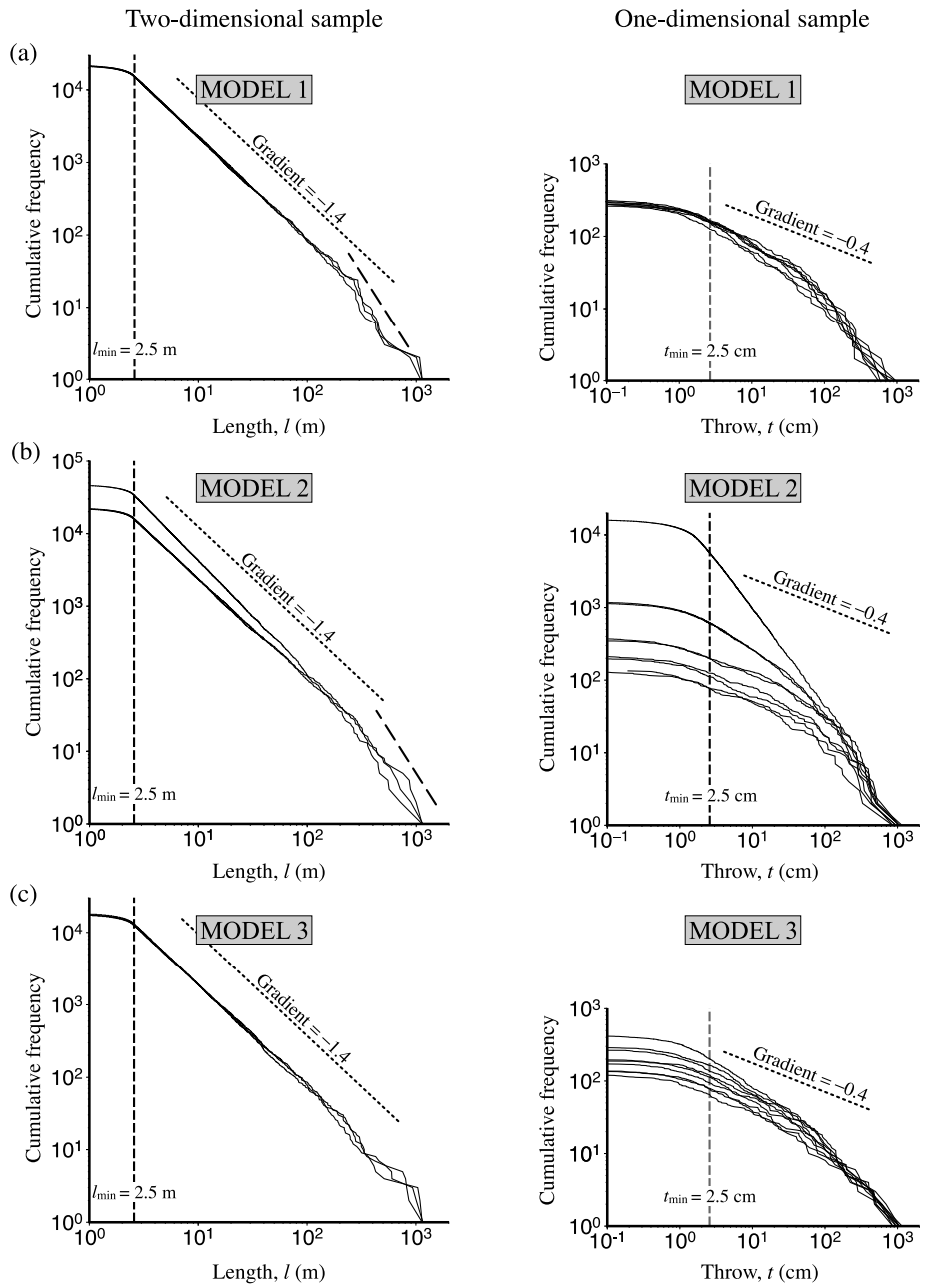


Fig. 11. Log–log plots of the cumulative frequency function against fault length, $l$, (m) and fault throw, $t$, (cm) for 2D and 1D subsamples, respectively, of the 3D fault damage zone models in the case of $D_3 = 2.4$: (a) model 1 (random spatial location of faults), (b) model 2 (simple clustering technique), and (c) model 3 (hierarchical clustering technique). The dotted lines for the 2D and 1D plots indicate the gradients $-1.4$ and $-0.4$, respectively, corresponding to a reduction of 1 or 2 with respect to the $D_3$ power law exponent. Multiple lines correspond to the three 2D samples and the (a) seven and ((b), (c)) nine 1D samples.

a shallowing of the slope at small scales (truncation) and a steepening of the slope at large scales (censoring). In addition, the slope of the cumulative distribution of a power law population steepens at large scales due to the upper cut-off imposed by the size of the sample (Bonnet et al., 2001). Although this effect can be avoided by using the density distribution, the cumulative distribution has been most commonly used in the literature since it generates a smoother trend. In the cumulative distribution, this effect reduces the segment of the graph over which the exponent can reliably be estimated. In some cases, the graph of a subsample from a power law population can become dominated by these effects, so that it becomes a curve with no significant straight line segment. In these cases, the subsamples cannot be used to estimate the power law exponent and, moreover, cannot be used to infer the nature of the parent population.

An analysis of the results of the 2D and 1D subsampling of fault arrays produced using the three spatial fault damage zone models, for $D_3 = 1.6$ to 2.8, has been made. In these subsamples, the segments of the graph where a straight line is appropriate has been determined graphically, which is a

commonly used method in the literature. In doing this, the limitations imposed by the 3D model have been taken into account. The random sample of faults from the 3D length population of the model was found to follow a power law accurately up to fault lengths of around 500 m (Fig. 9), which thus provides an upper limit to any straight line segment expected in a subsample. At small scales, the 3D population has a lower limit of a fault length of $l_{min} =$ 2.5 m, which corresponds to a throw of 2.5 cm. Lengths smaller than 2.5 m and throws less than 2.5 cm are therefore under-represented. In order to test the robustness of the graphical technique, three different subsampled populations have been analysed to determine the variation in the predicted slope, using a running average between triplets of points, and these are shown in Fig. 12. A straight line segment is considered to be significant when the slope stays constant (allowing for slight variations) over one order of magnitude or more of the measured length or throw (Fig. 12a and b). However, in some cases the slope is seen to steadily increase with the measured length or throw (Fig. 12c), indicating that no straight line segment exists and no power law relationship can be derived. It was found that the decision of whether a power law was appropriate, and the scale range over which it was valid, agreed well with the purely graphical method.

The results of exponent estimation from 1D and 2D subsamples for $D_3$ in the range 1.6–2.8 are summarised in Fig. 13. Fig. 13a and b shows that the number of faults sampled, $N_s$, varies widely according to both the model and the sample location. For the 2D subsamples (Fig. 13a), the number of faults sampled ranges from 1700 to 120,000, and for the 1D subsamples (Fig. 13b) this range is from 20 to 49,000. The effects of clustering in the fault spatial distribution (models 2 and 3) is to cause a general increase in the number of faults sampled as the exponent increases, whereas the random model shows less variation. The widest

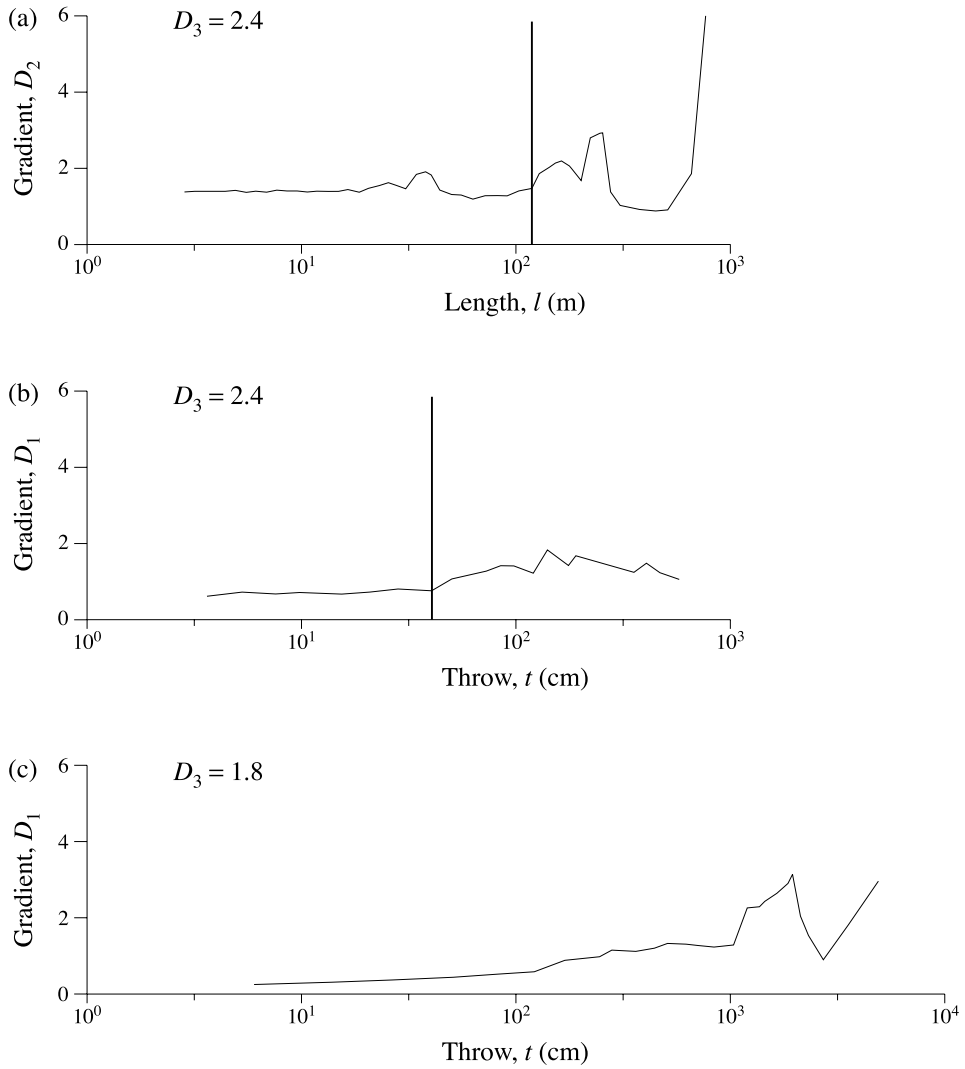


Fig. 12. Variations in the slope of log–log graphs of cumulative frequency distributions as functions of length or throw. The three examples show the range in behaviour observed in the 2D (fault length) and 1D (fault throw) subsamples of the 3D fault damage zone models. In (a) and (b) a straight line segment can be considered to exist over a scale range of one and one and a half orders of magnitude, respectively, to the upper limit indicated. In (c) the slope of the graph steadily increases with increasing throw and is not representative of a power law distribution.

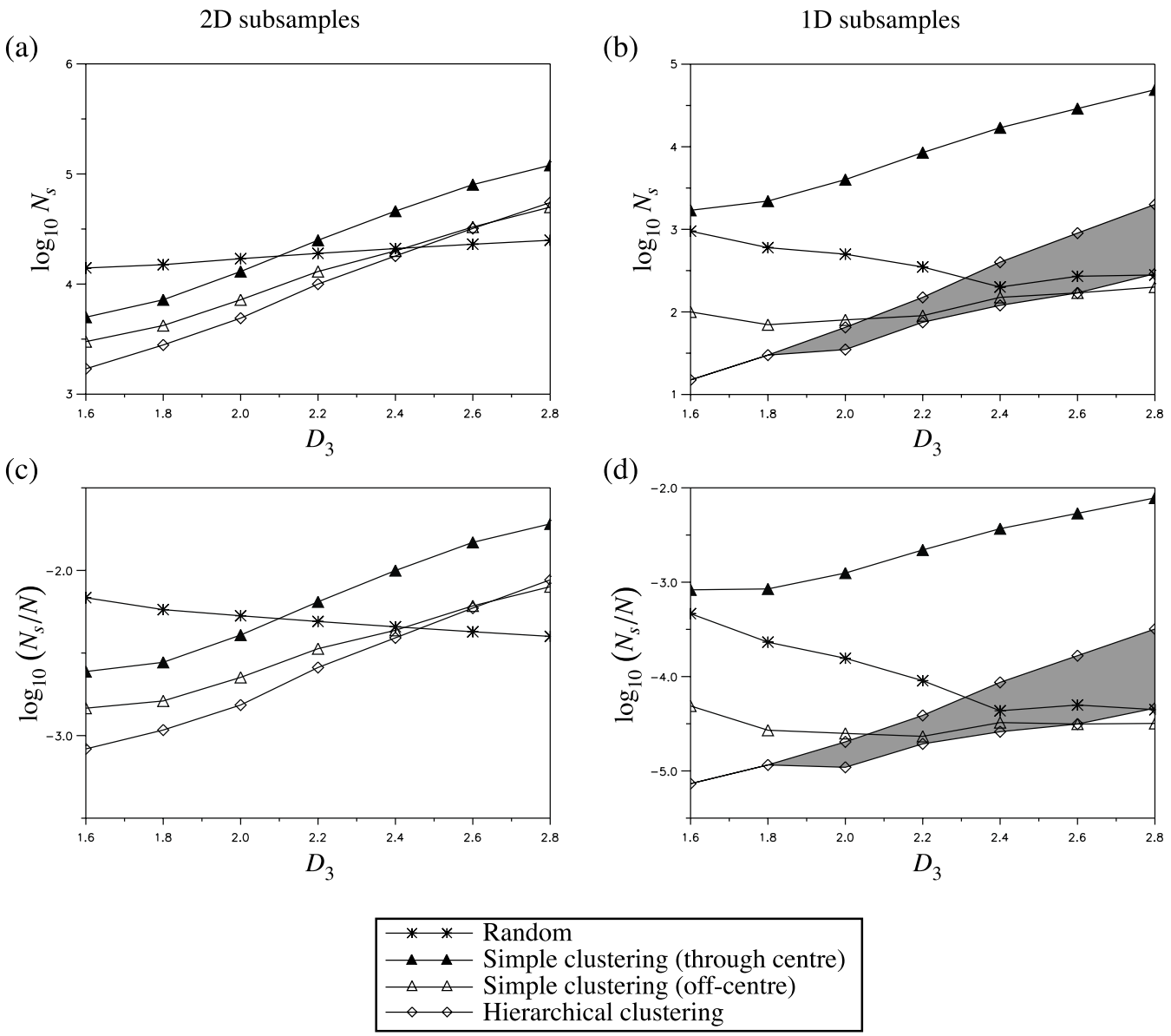


Fig. 13. Plots of ((a), (b)) the logarithm of the number of faults sampled, $N_s$, and ((c), (d)) the logarithm of the number of faults sampled as a proportion of the total number of faults, $N$, in the 3D model, for ((b), (d)) 1D and ((a), (c)) 2D subsamples. Models 2 and 3 (simple and hierarchical clustering models) show increasing sampled fault numbers as $D_3$ increases, whereas model 1 (random model) shows nearly constant to decreasing sampled fault numbers as $D_3$ increases. The shaded areas indicate a range of values for the plotted data.

range in the number of faults in subsamples occurs in model 2 (simple clustering model). Here, faults are closely clustered around the centre of the major fault, so that sample planes and lines away from the major fault centre encounter far fewer faults. Part of the variation in $N_s$ is due to the variations in the number of faults contained within the 3D models, $N$, since models with a higher exponent $D_3$ contain more faults to ensure the effective sampling of large faults. In order to eliminate this effect, the numbers of faults in 2D and 1D subsamples have been normalised with respect to the total number of faults, $N$, in the 3D model, and the variations in this ratio as a function of $D_3$ are shown in Fig. 13c and d. However, this plot displays very similar trends to Fig. 13a and b, showing that the variations are primarily due to the different spatial distributions of the models. Fig. 13c and d indicates that, as $D_3$ increases, the proportion of faults sampled increases for the clustered models (models 2 and 3), but decreases for the random model (model 1). As the $D_3$ exponent increases, the population contains a greater proportion of small faults. Since small faults have a smaller chance of being sampled by any plane or line, the proportion of faults sampled falls with increasing $D_3$ for the spatially random model. For the clustered model, however, the clustering of small faults around larger fault centres means that subsamples through such clusters record more than the expected number of small faults, so that the proportion of faults sampled tends to increase with $D_3$. This is most noticeable for the planes

passing through the centre of model 2, which has the greatest focusing of minor faults.

As illustrated by Fig. 11, the frequency distribution graphs range from straight lines to smooth curves, and thus a power law exponent cannot be estimated from all subsamples. It was found that 1D subsamples for $D_3$ between 1.6 and 2.2 could not be used to determine a power law exponent in all models, except for the sample through the major fault centre in model 2 (simple clustering model). This is caused, in part, by low fault numbers in these subsamples, particularly for the off-centre sample planes and lines in model 2 (simple clustering model). However, when $D_3 = 1.6$, the through-centre sample for model 2, which shows power law behaviour, contains a similar number of faults to the random model, for which an exponent could not be determined, indicating that the nature of the spatial clustering also has a significant effect on the subsample cumulative frequency distribution.

Fig. 14a and b shows the variation in the upper limit to the range over which straight line segments of the cumulative frequency distribution were found. The lower limit in all cases was 2.5 m (length) and 2.5 cm (throw), giving a range from one order of magnitude (considered to be the minimum acceptable range) to over two orders of magnitude. This range is generally greater for the clustering models (models 2 and 3) than for the random model (model 1). As the $D_3$ exponent increases, the range for all 2D subsamples (Fig. 14a) tends to converge to around one and a half orders of magnitude. However, for the 1D line subsamples (Fig. 14b), the through-centre case for model 2 (simple clustering) and model 3 (hierarchical clustering) exhibit higher ranges in comparison with the model 1 (random) and off-centre cases for model 2 (simple clustering). Thus, clustering appears to increase the range of validity of the power law distribution within the subsamples.

Fig. 14c and d shows the range of observed $D_1$ and $D_2$ exponents and their dependence on the $D_3$ value derived from the 2D and 1D subsamples, respectively. In the case of the models with clustering (models 2 and 3), some of the subsamples exhibited a range of slopes for the same $D_3$ value, showing that the location of the sample plane or line has a significant impact on the nature of the subsampled distribution. In particular, the off-centre cases of model 2 (simple clustering) show lower exponent values than the through-centre cases, for both the 2D and 1D subsamples. Model 3 (hierarchical clustering) also indicates a range of exponents for 1D cases for higher values of $D_3$ ($D_3 = 2.4$ to 2.8).

As $D_3$ increases, there is generally a corresponding increase in the derived $D_1$ and $D_2$ subsample exponents (Fig. 14c and d). In the 2D subsampling of fault lengths, model 1 (random), the off-centre cases in model 2 (simple clustering) and model 3 (hierarchical clustering) follow the simple rule that $D_2 = D_3 - 1$. However, the through-centre case for model 2 (simple clustering) shows exponents that are consistently and significantly higher than this simple relationship would predict, with discrepancies of up to 0.15. In the 1D subsampling of fault throws, many of the subsamples show exponents that differ significantly from the simple relationship $D_1 = D_3 - 2$, which is only approximated by some of the samples from model 1 (random), the off-centre cases from model 2 (simple clustering) and model 3 (hierarchical) for higher values of $D_3$ ($D_3 = 2.4$ to 2.8). Discrepancies between the observed exponents and this simple relationship are more extreme than for 2D sampling, with the through-centre case of model 2 (simple clustering) showing exponents around one greater than that predicted. This is caused by the extreme clustering within this model, so that, through the centre of the major fault, the throws of small faults are sampled to a larger extent than expected, and the sample resembles that expected from a 2D subsample.

## 7. Summary and discussion

Three-dimensional, stochastic models representing the internal structure of fault damage zones have been created, based upon observations from fault damage zones in siliclastic rocks. These models incorporate power law fault length distributions, preferred orientations and random to clustered spatial distributions. Three basic model types, corresponding to three types of spatial distribution, have been generated. These models have spatially random faults (model 1), a simple clustered distribution in which the smaller faults are focused around the major fault (model 2), and a hierarchically clustered model in which the smaller faults are clustered around the larger faults throughout the fault damage zone (model 3). Observations from outcrops suggest that faults tend to have clustered distributions within the fault damage zones, and, from a comparison of the frequency of faults across natural faults with the three models, it is suggested that the hierarchical model (model 3) provides the best representation of nature.

In practice, data is seldom available in three dimensions and the fault characteristics, such as the length and throw distributions, must be deduced from 2D sections, such as maps of outcrops or seismic horizons, or from 1D sections derived from line samples in outcrop, cores, bore hole logs, or horizon displacements in seismic sections. The extrapolation from 1D and 2D information to 3D is of crucial importance for providing an understanding of the fault network geometry. The three fault damage zone models have been used to investigate the effect of different parent 3D fault population characteristics on the nature of frequency distributions derived from 2D (fault length) and 1D (fault throw) subsamples. It was found that the resultant estimated fault length and throw power law distribution exponents depend on the 3D model fault size exponent, on the type of spatial clustering and on the location of the sample plane or line within the damage zone.

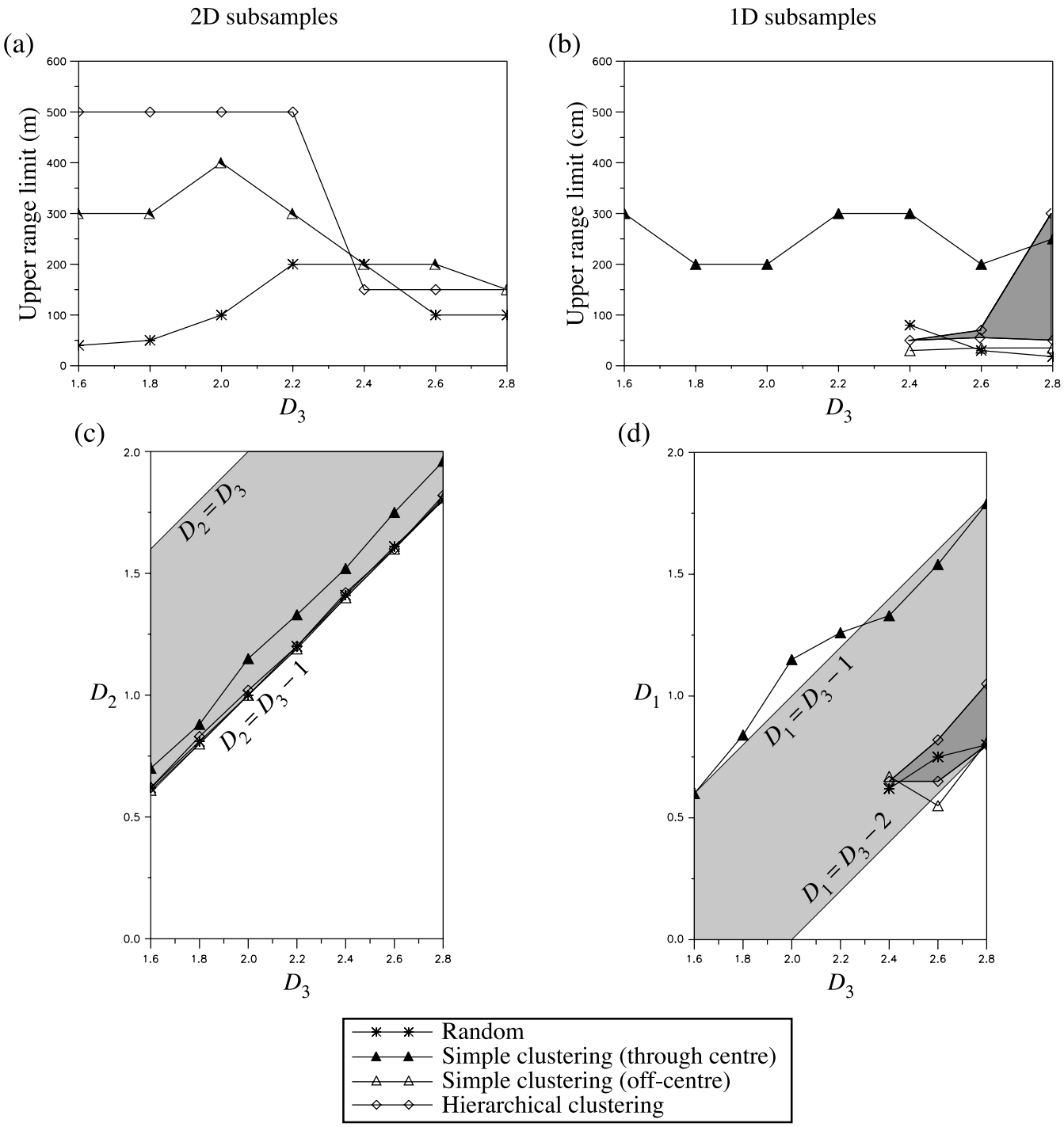


Fig. 14. ((a), (b)) Upper limit to the range over which the $D_1$ and $D_2$ exponents can be estimated. The lower limit is 2.5 m for 2D subsamples and 2.5 cm for 1D subsamples. The scale ranges over which exponents are estimated vary from one to one and a half orders of magnitude. ((c), (d)) Variation in the $D_1$ and $D_2$ exponents with the $D_3$ exponent for the three models. The pale shaded area represents the range between the simply-predicted relationships between the $D_1$, $D_2$ and $D_3$ exponents for a spatially random system of faults. The darker shaded area indicates a range of exponents found for model 3 (hierarchical clustering model).

Despite the power law nature of the parent 3D fault size–frequency distribution in all cases, 1D subsamples did not always show power law characteristics, particularly when the $D_3$ exponent was low ($D_3 = 1.6$ to 2.2). Some of these samples contained large numbers of faults (up to 600), so that these observations are unlikely to be due purely to small sample sizes, but are probably a result of model characteristics such as the fault length and spatial distributions. It seems that, in these cases, the effects of truncation and censoring have dominated, masking the power law nature of the underlying population. Thus, the presence of a parent power law length distribution need not necessarily be

apparent in 1D samples, particularly when the parent length exponent is low. Conversely, the absence of a straight line segment in a 1D cumulative frequency distribution of fault throw does not necessarily imply that the 3D fault population does not have power law characteristics.

In some of the 2D subsamples of fault length, the cumulative distribution appears to show two slopes, separated by a kink, with a steeper slope at larger scales (Fig. 11). There has been a tendency for such distributions to be interpreted as physically meaningful. However, here these cumulative distributions are derived from parent 3D populations that have power law size distributions with a single exponent. The change in the slope of the graph therefore does not reflect properties of the parent fault population. The most pronounced kinks are found for the clustered models and for low $D_3$ values ($D_3 = 1.6$ to 1.8), and may therefore be the result of uneven sampling of the population due to clusters of small faults around large faults. This illustrates how it may be misleading to interpret changes in the slope of the subsampled frequency distribution as physically meaningful without other supporting evidence, such as a change in the deformation mechanism from deformation bands to slip bands (Fossen and Hesthammer, 1997; Shipton and Cowie, 2001) or controlled by lithological layering from field observations.

For the case in which the fault location is random and independent of any other fault location, simple rules relate the exponents expected in 2D and 1D sections to those of the parent 3D population (Marrett and Allmendinger, 1991), namely $D_2 = D_3 - 1$ and $D_1 = D_3 - 2$. The presented models have shown that, in the 2D subsampling case, these simple rules are obeyed by most of the models, the only exception being the through-centre section of model 2 (simple clustering), which displays a consistently higher than expected exponent (discrepancy around 0.1). This is due to the clustering, which in this model is focused on the centre of the major fault. Thus, a 2D section through the centre-line of the major fault cuts more faults and, in particular, a higher proportion of small faults. The 1D sections show a wider range of behaviour and greater deviations from the simple rule that $D_1 = D_3 - 2$. Here, only some of the samples from model 1 (random), the off-centre cases from model 2 (simple clustering) and model 3 (hierarchical clustering) were found to approximate this simple relation, and then only for higher values of the $D_3$ exponent. In the case of the through-centre section of model 2 (simple clustering), the exponent lies around that expected for a 2D, rather than a 1D, section. This is again due to the concentration of minor faults around the centre of the major fault, so that 1D sections close to the centre of the major fault are likely to sample more small faults than expected within a random spatial distribution. Model 3 (hierarchical clustering) also shows some increase over the expected $D_1$ exponent by up to 0.25. In this model, the deviations from the simple rule are due to clusters throughout the damage zone rather than just a cluster centred on the major fault. Thus, higher than expected exponents occur in a number of locations through the fault damage zone, and not just close to the centre of the major fault. These clusters are not as pronounced as those developed by the simple clustering model, and so the effect on the exponent is less significant.

With respect to fault damage zones in nature, it is thought that model 3 (hierarchical clustering) probably provides the best representation. This tends to suggest that 2D sections can be expected to obey the simple rule that $D_2 = D_3 - 1$. However, results from 1D sections display a much more variable behaviour for this model, and the simple rule that $D_1 = D_3 - 2$ may give rise to an under-estimation of $D_3$ by up to 0.25. Thus, the use of 1D subsamples of faults to predict the 3D size–frequency distribution of faults should be undertaken with care, with some sensitivity analysis required on the range of fault numbers predicted at a given size. Our results suggest that spatial clustering based upon observed values of $D_2$ and $D_1$ will influence the fault population characteristics.

## 8. Conclusions

The key observations from the results of this study can be summarised as follows:

1. A hierarchical clustering scheme (model 3), in which small faults are clustered around larger faults throughout the fault damage zone, results in spatial distributions similar to those observed in nature.
2. The characteristics of 2D sections for fault length and 1D sections for fault throw depend on the parent fault size distribution and the spatial distribution of the 3D fault network.
3. For small values of the 3D power law fault size distribution exponent ($D_3 = 1.6$ to 2.2), the 1D subsample may fail to show power law characteristics. Thus, a lack of power law behaviour does not necessarily imply that the parent population is not power law.
4. Observed kinks in the cumulative frequency distribution of 2D fault lengths can arise from clustered spatial distributions and from a 3D parent population with a single power law size distribution. Thus, care should be taken not to interpret such kinks as physically meaningful without additional supporting evidence.
5. The simple rules whereby $D_2 = D_3 - 1$ and $D_1 = D_3 - 2$ are not always obeyed. The degree of clustering has a significant influence and tends to reduce these integer differences expected between the $D_1$, $D_2$ and $D_3$ exponents.
6. As a model for natural fault zones, the hierarchical damage zone model suggests that 2D sections through natural fault zones may obey the simple rule that $D_2 = D_3 - 1$ with only small deviations, but that 1D sections may depart from the rule that $D_1 = D_3 - 2$ by amounts of up to 0.25.

## Acknowledgements

The research was carried out under the projects at RDR (Rock Deformation Research, School of Earth Sciences, University of Leeds) which were sponsored by Arco, BG, BP, Elf, Mobil, Norsk Hydro, Pan Canadian Oil, Phillips, Saga Petroleum, Schlumberger Doll Research and Shell, and by the NERC Micro-to-macro thematic program (grant number GST /02/2506).

## References

Antonellini, M., Aydin, A., 1994. Effect of faulting on fluid flow in porous sandstones: petrophysical properties. American Association of Petroleum Geologists Bulletin 78, 355–377.

Antonellini, M., Aydin, A., 1995. Effect of faulting on fluid flow in porous sandstones: geometry and spatial distribution. American Association of Petroleum Geologists Bulletin 79, 642–671.

Aydin, A., 2000. Fractures, faults and hydrocarbon entrapment, migration and flow. Marine and Petroleum Geology 17, 797–814.

Baecher, G.B., Einstein, H.H., Lanney, N.S., 1977. Statistical descriptions of rock properties and sampling. In: Proceedings 18th Symposium of Rock Mechanics, American Institute of Mining Engineers, pp. 5C1.1–5C1.8.

Balberg, I., Binenbaum, N., 1983. Computer study of the percolation threshold in a two-dimensional anisotropic system of conducting sticks. Physical Review B28, 3799–3812.

Belfield, W.C., 1998. Incorporating spatial distribution into stochastic modelling of fractures: multifractals and Lévy-stable statistics. Journal of Structural Geology 20, 473–486.

Billaux, D., Chiles, J.P., Hestir, K., Long, J.C.S., 1989. Three-dimensional statistical modelling of a fractured rock mass—an example from Fanay–Augeres Mine. International Journal of Rock Mechanics, Mineral Science & Geomechanical Abstracts 26, 281–299.

Black, J.H., 1993. Hydrogeology of fractured rocks—a question of uncertainty about geometry. In: Memoirs XXIVth Congress of International Association of Hydrogeologists, Oslo, pp. 783–796.

Bonnet, E., Bour, O., Odling, N.E., Davy, P., Main, I., Cowie, P., Berkowitz, B., 2001. Scaling of fracture systems in geological media. Reviews of Geophysics 39, 347–383.

Borgos, H.G., Cowie, P.A., Dawers, N.H., 2000. Practicalities of extrapolating one-dimensional fault and fracture size–frequency distributions to higher-dimensional samples. Journal of Geophysical Research 105, 28,377–28,391.

Bour, O., Davy, P., 1999. Clustering and size distribution of fault patterns: theory and measurements. Geophysical Research Letters 26, 2001–2004.

Caine, J.S., Evans, J.P., Forster, C.B., 1996. Fault zone architecture and permeability structure. Geology 24, 1025–1028.

Childs, C., Walsh, J.J., Watterson, J., 1990. A method for estimation of the density of fault displacements below the limits of seismic resolution in reservoir formations. In: Buller, A.T., Berg, E., Hjelmeland, O., Kleppe, J., Torsaeter, O., Aasen, J.O. (Eds.), North Sea Oil and Gas Reservoirs II, Graham & Trotman, London, pp. 309–318.

Childs, C., Watterson, J., Walsh, J.J., 1995. Fault overlap zones within developing normal fault systems. Journal of the Geological Society of London 152, 535–549.

Collier, R.E., 1989. Tectonic evolution of the Northumberland basin; the effects of renewed extension upon an inverted extensional basin. Journal of the Geological Society of London 146, 981–989.

Cowie, P.A., Scholz, C.H., 1992a. Physical explanation for the displacement–length relationship of faults using a post-yield fracture mechanics model. Journal of Structural Geology 14, 1133–1148.

Cowie, P.A., Scholz, C.H., 1992b. Displacement–length scaling relationships for faults: data synthesis and discussion. Journal of Structural Geology 14, 1149–1156.

Cowie, P.A., Knipe, R.J., Main, I.G. (Eds.), 1996. Scaling Laws for Fault and Fracture Populations—Analyses and Applications. Journal of Structural Geology 18.

Dawers, N.H., Anders, M.H., 1995. Displacement–length scaling and fault linkage. Journal of Structural Geology 17, 607–614.

Dawers, N.H., Anders, M.H., Scholz, C.H., 1993. Growth of normal faults: displacement–length scaling. Geology 21, 1107–1110.

Dershowitz, W.S., Einstein, H.H., 1988. Characterizing rock joint geometry with joint system models. Rock Mechanics and Rock Engineering 21, 21–51.

Dershowitz, W.S., Eiben, T., Wadleigh, E., Cladouhos, T., 1998. Discrete feature network approaches for enhanced oil recovery. International Journal of Rock Mechanics, Mineral Science & Geomechanical Abstracts 35, 550.

Dugdale, D.S., 1960. Yielding of steel sheets containing slits. Journal of Mechanics and Physics of Solids 8, 100–104.

Fisher, Q.J., Knipe, R.J., 1998. Fault sealing processes in siliciclastic sediments. In: Jones, G., Fisher, Q.J., Knipe, R.J. (Eds.), Faulting, Fault Sealing and Fluid Flow in Hydrocarbon Reservoirs. Geological Society, London, Special Publications 147, pp. 117–134.

Fossen, H., Hesthammer, J., 1997. Geometric analysis and scaling relations of deformation bands in porous sandstone from the San Rafael Desert, Utah. Journal of Structural Geology 19, 1479–1493.

Foxford, K.A., Walsh, J.J., Watterson, J., Garden, I.R., Guscott, S.C., Burley, S.D., 1998. Structure and content of the Moab Fault Zone, Utah, USA, and its implications for fault seal prediction. In: Jones, G., Fisher, Q.J., Knipe, R.J. (Eds.), Faulting, Fault Sealing and Fluid Flow in Hydrocarbon Reservoirs. Geological Society, London, Special Publications 147, pp. 87–103.

Gabrielsen, R.H., 1990. Characteristics of joints and faults. In: Barton, N., Stephansson, O. (Eds.), Proceedings International Symposium on Rock Joints, ISRM, Loen, Norway, pp. 11–17.

Gillespie, P.A., Walsh, J.J., Watterson, J., 1992. Limitations of dimension and displacement data from single faults and the consequences for data analysis and interpretation. Journal of Structural Geology 14, 1157–1172.

Gillespie, P.A., Howard, C.B., Walsh, J.J., Watterson, J., 1993. Measurement and characterisation of spatial distributions of fractures. Tectonophysics 226, 113–141.

Heffer, K.J., Bevan, T.G., 1990. Scaling relationships in natural fractures: data, theory and applications. Society of Petroleum Engineers Paper 20981, 369–376.

Hestir, K., Chiles, J.-P., Long, J., Billaux, D., 1987. Three-dimensional modelling of fractures in rock: from data to a regionalized parent–daughter model. In: Evans, D.D., Nicholson, T.J. (Eds.), Flow and Transport Through Unsaturated Fractured Rock. Geophysical Monograph 42, AGU, Washington DC, pp. 133–140.

Jackson, P., Sanderson, D.J., 1992. Scaling of fault displacements from the Badajoz–Cordoba shear zone, SW Spain. Tectonophysics 210, 179–190.

Jones, G., Fisher, Q.J., Knipe, R.J. (Eds.), 1998. Faulting, Fault Sealing and Fluid Flow in Hydrocarbon Reservoirs. Geological Society, London, Special Publications 147.

Knipe, R.J., Fisher, Q.J., Jones, G., Clennell, M.R., Farmer, A.B., Harrison, A., Kidd, B., McAllister, E., Porter, J.R., White, E.A., 1997. Fault seal analysis: successful methodologies, application and future directions. In: Møller-Pedersen, P., Koestler, A.G. (Eds.), Hydrocarbon Seals: Importance for Exploration and Production. NPF Special Publication 7, Elsevier, Singapore, pp. 15–40.

Knipe, R.J., Jones, G., Fisher, Q.J., 1998. Faulting, fault sealing and fluid flow in hydrocarbon reservoirs: an introduction. In: Jones, G., Fisher, Q.J., Knipe, R.J. (Eds.), Faulting, Fault Sealing and Fluid Flow in Hydrocarbon Reservoirs. Geological Society, London, Special Publications 147, pp. vii–xxi.

Knott, S.D., Beach, A., Brockbank, P.J., Lawson Brown, J., McCallum, J.E., Welbon, A.I., 1996. Spatial and mechanical controls on normal fault populations. Journal of Structural Geology 18, 359–372.

Koch, G.S., Link, R.F., 1970. Statistical Analysis of Geological Data, Vol. I, Dover, New York, p. 375.

Lindsey, R.W., Rothrock, D.A., 1995. Arctic sea ice leads from advanced very high resolution radiometer images. Journal of Geophysical Research 100C, 4533–4544.

Long, J.C.S., Rener, J.S., Wilson, C.R., Witherspoon, P.A., 1982. Porous media equivalents for networks of discontinuous fractures. Water Resources Research 18, 645–658.

McGrath, A.G., Davidson, I., 1995. Damage zone geometry around fault tips. Journal of Structural Geology 17, 1011–1024.

Marrett, R., Allmendinger, R., 1991. Estimates of strain due to brittle faulting: sampling of fault populations. Journal of Structural Geology 13, 735–738.

Martel, S.J., Boger, W.A., 1998. Geometry and mechanics of secondary fracturing around small three-dimensional faults in granitic rock. Journal of Geophysical Research 103, 21299–21314.

Nicol, A., Watterson, J., Walsh, J.J., Childs, C., 1996. The shapes, major axis orientations and displacement patterns of fault surfaces. Journal of Structural Geology 18, 235–248.

Odling, N.E., 1997. Scaling and connectivity of joint systems in sandstones from western Norway. Journal of Structural Geology 19, 1257–1271.

Odling, N.E., Gillespie, P.A., Bourgine, B., Castaing, C., Chilés, J.P., Christiansen, N.P., Eeles, M., Fillion, E., Genter, A., Madsen, L., Olsen, C., Trice, R., Walsh, J.J., Watterson, J., 1999. Variations in fracture system geometry and their implications for fluid flow in fractured hydrocarbon reservoirs. Petroleum Geoscience 5, 373–384.

Pickering, G., Bull, J.M., Sanderson, D.J., 1995. Sampling power law distributions. Tectonophysics 248, 1–20.

Pickering, G., Bull, J.M., Sanderson, D.J., 1996. Scaling of fault displacements and implications for the estimation of sub-seismic strain. In: Buchanan, P.G., Nieuwland, D.A. (Eds.), Modern Developments in Structural Geology, Interpretation, Validation and Modelling. Geological Society, London, Special Publications 99, pp. 11–26.

Pollard, D.D., Segall, P., 1987. Theoretical displacements and stresses near fractures in rock: with applications to faults, joints, veins, dikes, and solution surfaces. In: Atkinson, B.K., (Ed.), Fracture Mechanics of Rock, Geology Series, Academic Press, pp. 277–347.

Rippon, J.H., 1985. Contoured patterns of the throw and hade of normal faults in the Coal Measures (Westphalian) of north-east Derbyshire. Proceedings of the Yorkshire Geological Society 45, 147–161.

Robinson, P.C., 1983. Connectivity of fracture systems—a percolation threshold approach. Journal of Physics A 16, 605–614.

Sammis, C.G., Osborne, R.H., Anderson, J.L., Banerdt, M., White, P., 1986. Self-similar cataclasis in the formation of fault gouge. Pure and Applied Geophysics 124, 53–78.

Scholz, C.H., Cowie, P.A., 1990. Determination of total strain from faulting using slip measurements. Nature 346, 837–838.

Shipton, Z.K., Cowie, P.A., 2001. Analysis of three-dimensional damage zone development over a micron to km scale range in the high-porosity Navajo sandstone, Utah. Journal of Structural Geology 23, 1825–1844.

Shipton, Z.K., Evans, J.P., Robeson, K., Forster, C.B., Snelgrove, S., 2002. Structural heterogeneity and permeability in faulted eolian sandstone: implications for subsurface modelling of faults. American Association of Petroleum Geologists Bulletin 86, 863–883.

Sibson, R.H., 1992. Implications of fault valve behaviour for rupture nucleation and recurrence. Tectonophysics 211, 283–293.

Skamvetsaki, A., 1994. Spatial characterization of fault zones in yellow Permian sandstones, Northumberland, NE England. Extended abstract, Tectonic Studies Group Meeting on Fault Populations. Geological Society, London, 19–20 October, p. 85.

Steen, Ø., Andresen, A., 1999. Effects of lithology on geometry and scaling of small faults in Triassic sandstones, East Greenland. Journal of Structural Geology 21, 1351–1368.

Walsh, J.J., Watterson, J., 1988. Analysis of the relationship between displacements and dimensions of faults. Journal of Structural Geology 10, 239–247.

Watterson, J., 1986. Fault dimensions, displacements and growth. Pure and Applied Geophysics 124, 365–373.

Watterson, J., Walsh, J.J., Gillespie, P.A., Easton, S., 1996. Scaling systematics of fault sizes on a large range fault map. Journal of Structural Geology 18, 199–214.